EarthArXiv Coversheet

Andrew Gunn[1,*]

[1]School of Earth, Atmosphere & Environment, Monash University, Clayton, Victoria, Australia

[*]a.gunn@monash.edu

This preprint is in review at *Nature Communications* and has undergone no rounds of peer review.

[*]a.gunn@monash.edu

This preprint is in review at *Nature Communications* and has undergone no rounds of peer review.

The distribution of Earth's wind-blown sand dunes

Andrew Gunn[1,*]

[1]School of Earth, Atmosphere & Environment, Monash University, Clayton, Victoria, Australia

[*]a.gunn@monash.edu

Abstract

Sand dunes develop when there is a source of sediment and wind capable of saltating that sediment. Dune morphology and occurrence can then be used to infer the distribution of sediment sources and climate conditions during their formation. This is particularly useful for inference of past climate from relict dunes or the sedimentary record, and for climate conditions where direct observation is challenging on Earth or other planets. However, to date, there has been no complete and accurate global map of the occurrence of Earth's sand dunes with distinguishable morphologies. Here we present that map and use it to demonstrate quantitatively that in arid environments dune presence is mostly explained by convergent transport and source proximity, whereas in more humid climates wind strength is an additional constraint. By limiting our analysis to dunes with morphologies discernible from global publicly available imagery and topographic data, we produce a consistent dataset which can be used to infer myriad aspects of geology and climate, and improve understanding of processes in, and development of, aeolian landscapes. We provide an example, using the orientation of barchan dunes, to demonstrate a trade-off between inference of sediment and wind characteristics.

Main text

Aeolian dune fields are landscapes on Earth's surface that are often associated with environments of friable sandstones and arid, windy climates such as the Sahara. There are, however, many dunes in contrasting environments like temperate coastal[1] or high-latitude permafrost[2] landscapes. Understanding of how dune fields develop in such a wide variety of climactic and geologic conditions has been hampered by a lack of in situ data from these typically inhospitable and inaccessible landscapes, but also simply because, unlike Mars[3], no complete, global map of their locations exists. Despite this absence of data, past work in well-chosen case studies[4] has established a prevailing view that criteria for aeolian dune field development are a sand source (e.g., sedimentary surface lithologies), sand availability (e.g., lack of vegetation cover), and potential sand transport (e.g., winds that can saltate that sand). Contemporary publicly available, global climate[5,6], surface imagery, and elevation[7] datasets allow us to reassess what conditions necessitate aeolian dunes.

Quantitative understanding of these conditions is significant for predicting how landscapes respond to climate and, in turn, what risk climate-driven desertification poses to infrastructure and agriculture in the future[8]. Contradictory, bold predictions of dune development through contemporary and future aridity[9] and wind[10,11] demonstrate this risk assessment is highly uncertain. This uncertainty can partly be attributed to incomplete data on dune presence. Additionally, robust constraints on present-day factors conducive to dune development allow us to develop frameworks for better inference of paleoclimate from the aeolian stratigraphic record[12]. Beyond their presence alone, dune morphology reveals myriad climate and geology information (e.g., wind regime and sediment supply[13]), however development and testing of theories linking morphology to boundary conditions would benefit from access to larger, unbiased data.

In this study we produce an exhaustive map of Earth's dunes and, using climate reanalysis[5,6], geologic mapping[14], remotely sensed data[6], and observational data[15], evaluate what leads to their spatial distribution. Then, with a novel approach to predicting dune orientation, we use this map to demonstrate that there are regions of Earth's surface where sediment characteristics can be inferred from dune morphology, illustrating its benefit for future research.
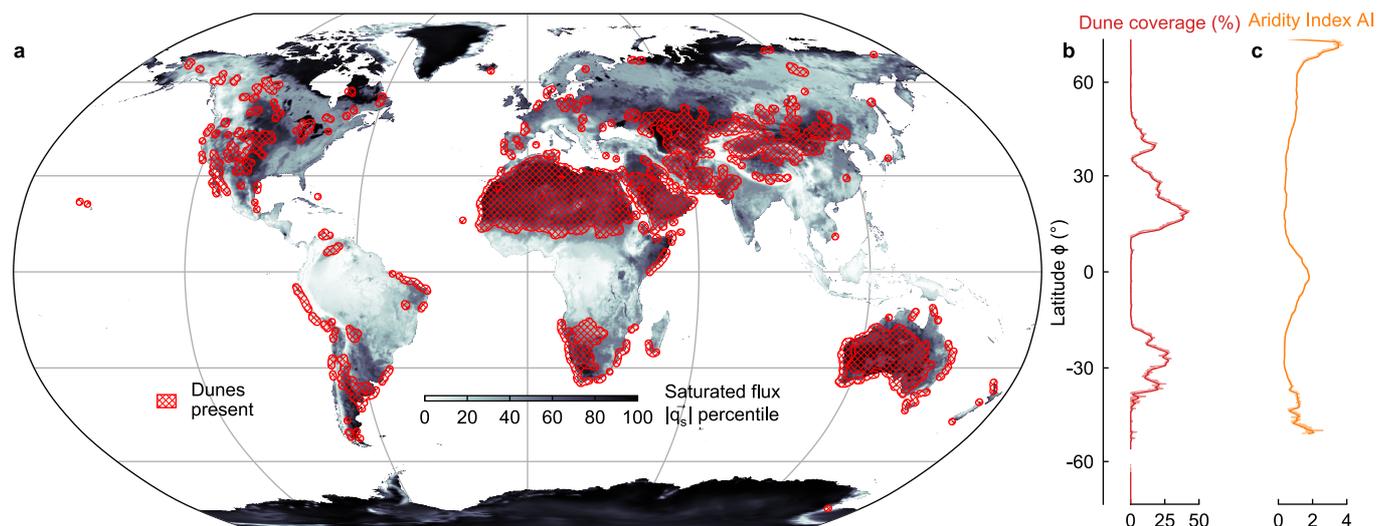

Fig. 1: Distribution of Earth's wind-blown sand dunes with discernible morphologies. a, Dune presence hatched in red on a world map (ESRI:54030) of the area-weighted percentile of average saturated sand flux magnitude $|\overline{q_s}|$ (m²/yr) for the period 1950-2024. **b**, The zonally averaged dune coverage fraction (%), where coverage is defined in 0.1°x0.1° grid cells with respect to land cover. **c**, The zonally averaged Aridity Index[5] AI, which is left undefined in Antarctica. In **b** & **c** the dark line is a 1° rolling meridional average whereas the light shading is at 0.1° resolution. Note that, for clarity, dune locations **a** are padded by a 100-km radial buffer.

Conditions for dune formation

Using satellite imagery and derived surface elevation data[6], we identify the presence of dunes in 0.1°x0.1° grid squares over Earth's surface, aided by past mapping efforts (Methods M1). We find dunes present on 7.8% of the surface and all continents (Fig. 1a), with relatively high prevalence of dunes in the lower mid-latitudes (Fig. 1b), broadly consistent with the inverse of the Aridity Index[5] meridional signal (Fig. 1c, Methods M2). The Aridity Index AI is the ratio of precipitation over potential evapotranspiration, and therefore lower when conditions are more arid. Aside

from arid conditions, a common idea is that fast winds necessitate dune presence. In Fig. 1a we plot dune presence over percentiles of the average magnitude of saturated sand flux, $|\overrightarrow{q_s}|$, calculated using reanalysis data (Methods M3). Saturated sand flux is the transport rate when there is complete sand availability and increases with wind speed above the threshold required to move sand[16,17]. We see qualitatively that large dune fields are generally co-located with elevated $|\overrightarrow{q_s}|$, however there are many regions devoid of dunes where saturated flux is higher, and where they are present and saturated flux is low. Neither AI nor $|\overrightarrow{q_s}|$ alone can explain the distribution of dunes.

Over the last century it has been established[16,18] that dunes prevail when both sediment is available and saturated flux is sufficient. AI correlates well with how vegetation presence[18,19] and other major factors[20] inhibit open, loose sand surface cover, thus making it a reasonable proxy for the inverse of sediment availability. In Fig. 2a-i we plot example grid cells across Earth where dunes exist in unimodal sand transport regimes (Methods M4) to illustrate how dune morphology depends on AI and $|\overrightarrow{q_s}|$. The genetic morphological transition from parabolic dunes at high AI to barchans at low AI is clear, while subtler quantitative morphologic transitions are sensitive to $|\overrightarrow{q_s}|$[21,22]. Because the dune presence map is close to exhaustive (Methods M1), we can plot the fractional coverage of dunes for binned values of AI and $|\overrightarrow{q_s}|$ (Fig. 2k), finding that dunes are uncommon in humid, stagnant climates. A well-chosen equality, $\log_{10} AI < 10^{-11/5}|\overrightarrow{q_s}| - 4/5$ (Methods M5, Extended Data Fig. 1), delineates 93% of dune coverage occurring in just 25% of Earth's terrestrial surface. This relation improves on the accuracy and applicability of prior dune mobility index thresholds[18,23] (Supplementary Text 2). Fig. 2k also shows that dunes are generally most prevalent relative to other land regions when saturated flux is moderate, not high (56 m^2/yr is the 75th percentile $|\overrightarrow{q_s}|$, Extended Data Fig. 2). This can be explained by the near absence of sand dunes on glacial, windy Antarctica and Greenland, whereas the prevalence at extreme fluxes occurs mostly where consistent, fast onshore winds over beach sands produce transgressive dunes[24].

The saturated flux divergence, $\nabla \cdot \overrightarrow{q_s}$ (m/kyr; (Methods M6), is another distinct, highly relevant factor required to explain the presence of dunes. Until recently[12,25], quantification of $\nabla \cdot \overrightarrow{q_s}$ (which is negative for deposition and positive for erosion) has not been employed to understand the development of dune fields, despite clear qualitative descriptions of its importance and widespread use at the landform scale[16,21]. Dune fields are less likely to occur when there is more sand leaving a region than entering, regardless of if there is a sediment source, availability of sand, and above-threshold winds. Here we demonstrate this in Africa (Fig. 3), where we assume that previously-mapped[14] surficial lithologies of aeolian sediments are source regions (Methods M7). Fig. 3a shows the Aridity Index AI, surficial aeolian sediment sources, and dune presence over the continent, demonstrating that there are arid areas of the Sahara and Sahul where saturated sand flux is more than sufficient for dune development
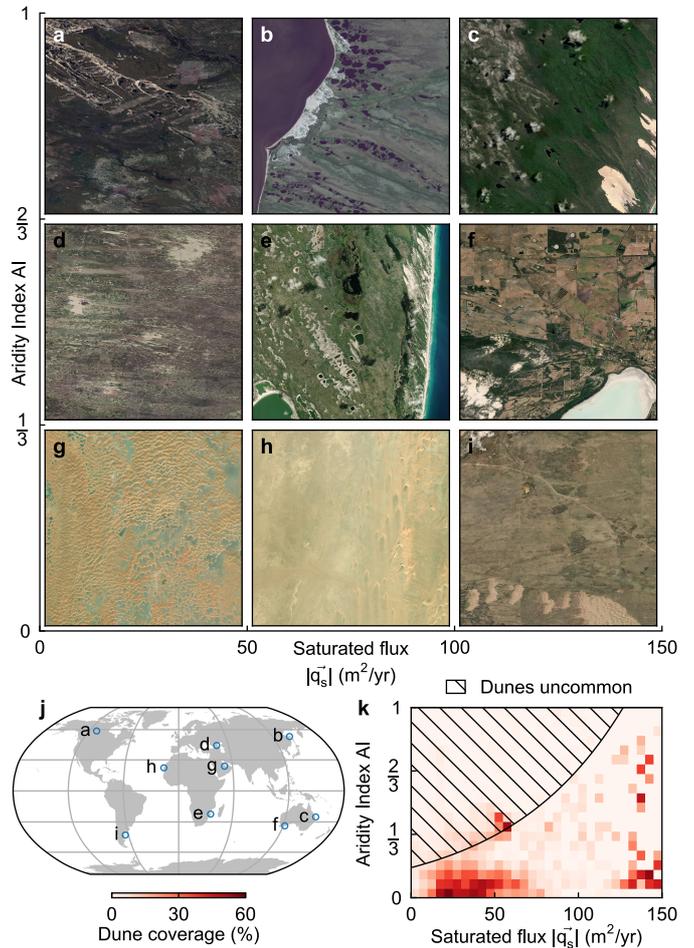

Fig. 2: Dependence of dune presence and form on key boundary conditions. a-i, Example dune morphologies in approximately unimodal transport regimes (RDP/DP>0.2; Methods M4) in binned values of the average saturated sand flux magnitude $|\overrightarrow{q_s}|$ (m^2/yr) and Aridity Index AI, where each panel is 0.1°x0.1° (EPSG:4326), north is up, and **j** shows their locations (ESRI:54030). **k**, The area-weighted dune coverage fraction (%), where coverage is defined in 0.1°x0.1° grid cells with respect to land cover, for bins of $|\overrightarrow{q_s}|$ and AI with the relation $\log_{10} AI > 10^{-11/5}|\overrightarrow{q_s}| - 4/5$ hatched. Image credit: Bing (**b,c,e,f,g,h&i**) and Google Satellite (**a&d**) Maps.

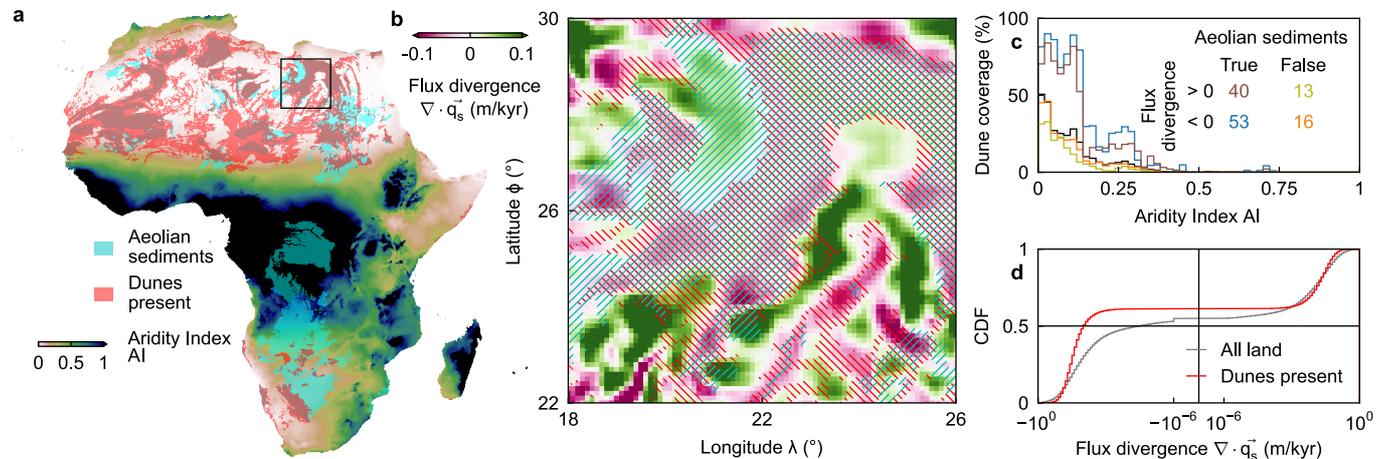**Fig. 3: Conditions for dune presence in Africa. a**, A map (EPSG:4326) of the Aridity Index AI in Africa with surficial aeolian sediment lithology[14] (cyan) and dune presence (red) overlayed, and the region of **b** outlined (black). **b**, The average saturated flux divergence $\nabla \cdot \overrightarrow{q_s}$ (m/kyr), where negative values (pink) imply deposition, in a subregion over the Zaltan, Great Sand Sea, and Calanscio dune fields with the same overlays as **a** (diagonally stitched for clarity). **c**, The area-weighted dune coverage fraction (%) for Africa, where coverage is defined in 0.1°x0.1° grid cells with respect to land cover for bins of AI, conditioned on where there is or is not surficial aeolian sediment and $\nabla \cdot \overrightarrow{q_s}$ implies erosion or deposition. The inset confusion matrix, where coloured numbers match their respective lines, shows the total dune coverage (%) for that condition, while the black line is for the whole continent. **d**, The area-weighted cumulative distribution function of $\nabla \cdot \overrightarrow{q_s}$ for Earth, for all land (grey) and where dunes are present (red). Note that the abscissa scale and bins are in symmetric log-space, linear for $|\nabla \cdot \overrightarrow{q_s}|<10^{-6}$ m/kyr.

(Fig. 1a) yet there are no dunes. Fig. 3b shows an example where erosional $\nabla \cdot \vec{q_s}$ inhibits the development of dunes over exposed source regions between depositional Zaltan and Great Sand Sea dune fields. To quantify the importance of $\nabla \cdot \vec{q_s}$, we plot the dune coverage with respect to land conditional on underlying aeolian sediment source presence, the sign of $\nabla \cdot \vec{q_s}$ (i.e., erosional or depositional), and AI (Fig. 3c). We find that dunes are present in most depositional source regions, regardless of aridity, and that for almost all AI bins, dunes are more prevalent in depositional rather than erosional regions regardless of if there is a source or not. While dune presence is more sensitive to underlying sediment source and AI, knowledge of large-scale gradients in saturated flux is necessary to understand the distribution of sand dunes in Africa. Furthermore, across Earth we find that dunes are overrepresented in depositional regions, with the majority occurring within regions in the top third of land's deposition rates (Fig. 3d).

Boundary condition inversion from morphology

These new quantitative explanations of dune occurrence aid in prediction of boundary conditions such as surficial sediment cover, surface wind divergence, and aridity, however far more geologic and climatic detail can be garnered from dune morphology[13,22,26]. With the prior results in hand, we provide—as an example of the utility of the new data we present—a novel insight on a popular additional climate constraint provided by aeolian landscapes. The horns of crescent-shaped barchan dunes point in the direction they migrate and therefore can be used to infer the direction unimodal, above-threshold winds blow[16,21,27]. Whereas in the section above and most studies[10,23,26] a representative value for threshold friction velocity u_t (m/s; which wind must exceed to move sand) is fixed, here we find the direction that barchan dunes migrate (accounting for the increased flux that occurs on steeper wind-facing slopes[26]; Methods M8), as a function of u_t. For loose, dry sand, this threshold is mostly controlled by sediment density and size[28]—major sedimentological characteristics of source rocks. It follows then that the u_t which produces the prediction closest to the observed dune orientation could be a proxy for geologic boundary conditions.

We illustrate this with example barchan and parabolic dunes in the Qaidam Basin, China (Fig. 4a), finding that the u_t where reanalysis wind data best-predicts their observed migration direction is ~0.35 m/s and there is a ~60° range in predicted directions, $\Delta_{0.1}^{0.4}\alpha_T$, for reasonable values of u_t (between 0.1 and 0.4 m/s; Fig. 4b). There is clear sensitivity of orientation to threshold in this example and, integrating over the complexity of the wind rose, a non-monotonic response. We represent this idea on a global scale using $\Delta_{0.1}^{0.4}\alpha_T$ (Fig. 4c), finding that in some places dunes on Earth would migrate in effectively the opposite direction if they were made of different sediment, while in large swaths of the planet their orientation would be essentially independent of geologic conditions. The inset of Fig. 4c plots the cumulative distribution functions of $\Delta_{0.1}^{0.4}\alpha_T$ conditional on land cover, dune presence, and predicted locations of barchan dunes[29] (Methods M9). These illustrate that dunes are overrepresented where their migration direction is insensitive to geologic conditions, and barchans even more so. The 75th percentile $\Delta_{0.1}^{0.4}\alpha_T$ for Earth's dunes is ~8.6°.
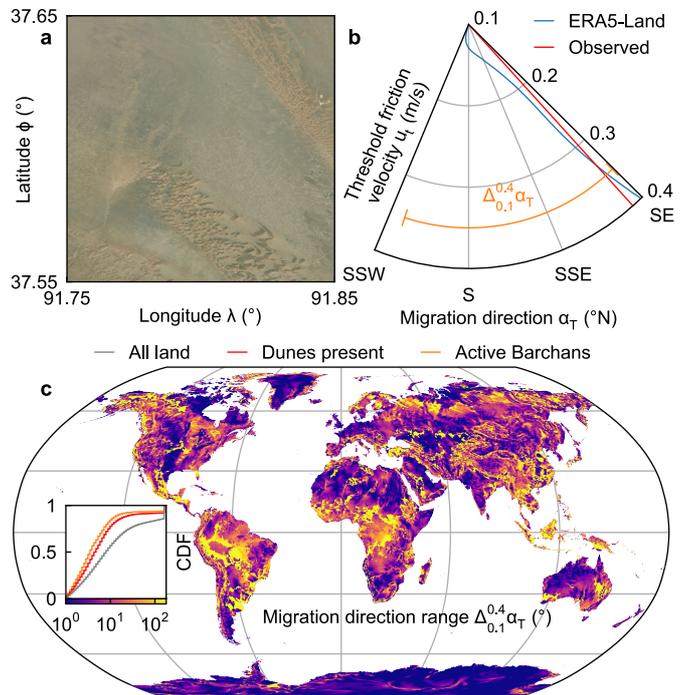

Fig. 4: Sensitivity of dune migration direction to surface conditions. a, Example imagery of unimodal dunes (EPSG:4326. Credit: Bing Maps). **b**, The dependence of the inferred migration direction α_T (°N) in **a** on a range of typical threshold friction velocities $0.1 < u_t < 0.4$ (m/s) (blue), the approximate observed direction (red) and the total range in possible α_T within this u_t range, $\Delta_{0.1}^{0.4}\alpha_T$ (°) (orange). **c**, The global distribution (ESRI:54030) of $\Delta_{0.1}^{0.4}\alpha_T$ (°; log-scale), with the area-weighted log cumulative distribution function of $\Delta_{0.1}^{0.4}\alpha_T$ for land (grey), dunes (red), and only active barchans[29] (Methods M8; orange) inset.

Implications for geomorphology and sedimentology

This analysis includes so-called relict dunes, i.e., aeolian landforms with discernible morphologies that are not considered active in the contemporary climate (e.g., covered by vegetation). This introduces bias—limited as these a small fraction of the dataset—to some results because, e.g., present-day aridity and flux divergence do not correspond to their formative conditions. Regardless, they are included as there is no clear threshold within the gradient of activity between relict, intermittently active, reactivated, and free dunes[30,31]. For example, many parabolic dunes are predominantly covered by vegetation yet migrate on decadal timescales[1,2], while other dunes may be imaged on years where vegetation is anomalously recovered from bushfires[32]. Furthermore, on longer timescales, debates exist on whether variability in dune development on centennial timescales (due to aspects of climate such as drought) overwhelms any glacial-interglacial signal[33]. Indeed, the large overlap between the younger distribution of dated aeolian sediment burial ages[15] where dunes are present and older distribution where they are not hints at this complexity (Extended Data Fig. 3). We anticipate that the data, ideas, and methods presented here to aid in developing more quantitative insights into dune formation over the Quaternary and inference of aeolian paleoclimate signals.

The quantification (Fig. 2k) of major advances in our qualitative understanding of the conditions for global dune-field development[4], in addition to evidence for the additional condition of negative flux divergence (Fig. 3b-d), will allow for more robust predictions of climate's role in environmental change, in the past, future, and on other planets. For example, aridity and wind predictions from simulations of climate over the 21st century from the Coupled Model Intercomparison Project can be fed into the relations identified in this paper (e.g., Extended Data Figs. 1 & 4) to guide our expectations of desertification, unifying approaches in recent studies which focus solely on wind climate[10,11] or aridity[34]. Furthermore, the dataset produced here serves as a foundation for targeted, exhaustive studies linking dune morphology (e.g., the diversity of parabolics[22] or barchans[21]) to detailed properties of climate (e.g., wind gusts[35]) and vegetation (e.g., growth rate[31]).

Despite these prospects for understanding the tight coupling between climate and landscapes, Fig. 4 illustrates how they can be hampered by a fundamental trade-off between inference of climate and geology from geomorphic signals. Inference of surface winds and aeolian sediment transport pathways on other planets[27] may, in places, be bias due to spatial heterogeneity in sediment characteristics, while uncertainties in paleowind directions inferred from aeolianite bedding[36] or relict dune orientation[37] attributable to sediment characteristics could be larger than

studied signals. On the other hand, in some places (e.g., Fig. 4a), if accurate wind climate data is available this approach offers an approach to recover source rock properties remotely alongside others (e.g., hyperspectral imagery[38]). Finally, this study raises planet-scale questions surrounding the correlation between dune field boundary conditions themselves, on instantaneous spatial scales or locally on geologic timescales, such as how tectonically-driven exposure of source-rocks shapes aeolian flux and its gradients spatially to feedback on relief, or how correlation between aridity and divergent surface flows[39] may minimize dune abundance on hydrologically-active planets.

Methods

M1. Dune mapping

The presence of dunes was identified in either satellite imagery (Google Satellite and Bing Maps basemaps; accessed 10/12/25-18/1/26) or 30-m topography (Copernicus Global Digital Surface Model[7]) derived from satellite imagery stereography. Mapping was conducted using projection EPSG:4326 (or EPSG:3857 at high latitudes) using QGIS. A grid square is classified as true for dune presence if part, all, or many dunes are contained within it. Dunes were identified at 1:30,000 scale (nominal), however a smaller scale was used to verify potential dune candidates found at this scale. Some dunes are identifiable only with imagery or topography, not both.

The process of identification was to first produce a global raster of 'False' values, where each square is centred on latitude-longitude points with 1 decimal point, such that presence is flagged within the square. For example, if point [-25.2, 137.4] is 'True', there is dune in the square [[-25.25, -25.15], [137.35, 137.45]]. Then by manually inspecting primary data (imagery and topography) and/or secondary sources (Supplementary Text 1), dunes were identified then marked as 'True' in the raster using QGIS plugin Serval. Secondary sources were used as vector or raster data if provided accessibly, or maps were georeferenced manually.

All identification of the 106,531 grid cells with dunes present was done manually using expert opinion. Some secondary sources use artificial intelligence methods[29], extrapolated correlations between multispectral satellite imagery and dune or sand presence[40], or manual identification[41]. These datasets are each of high value, however they can contain false positive and/or negatives, map at far finer or coarser scales, or map for a different purpose, therefore they were only used as guides. Since in practice this map was produced manually, from False to True, without assessing some regions (e.g., away from the coast in tropical equatorial landscapes), we anticipate it has almost zero false positives but has some false negatives. Further information on the mapping process, previously unreported dune fields, and definitions of dunes can be found in Supplementary Text 1.

M2. Aridity Index

The Aridity Index AI used in this study is the previously published "Global Aridity Index and Potential Evapotranspiration Database - Version 3.1"[5] based on FAO-56 Penman-Monteith equation for evapotranspiration. Here we use the average value for the period 1970-2000 and coarsen the dataset from 30 arcseconds to a 0.1° grid co-located with the ERA5-Land reanalysis grid.

M3. Saturated sand flux

The volumetric saturated sand flux $\overrightarrow{Q_s}$ (m²/s) is calculated as[17],

$$\overrightarrow{Q_s} = \begin{cases} \frac{C_q u_t \rho_f}{g \rho_s \phi_s}\left(\left(\frac{\overrightarrow{u_z}\kappa}{ln(z/z_0)}\right)^2 - u_t^2\right), & \frac{|\overrightarrow{u_z}|\kappa}{ln(z/z_0)} > u_t \\ 0, & \frac{|\overrightarrow{u_z}|\kappa}{ln(z/z_0)} \le u_t \end{cases},$$

with assumed constants (non-dimensional flux constant is $C_q = 5$, threshold friction velocity for saltation $u_t = 0.15$ m/s (unless otherwise stated), fluid (air) density $\rho_f = 1.2$ kg/m³, solid (sand) density $\rho_s = 2650$ kg/m³, gravity $g = 9.8$ m²/s, packing fraction $\phi_s = 0.6$, von Kármán's constant $\kappa = 0.41$, and roughness length $z_0 = 10^{-3}$ m, and hourly near-surface ($z = 10$ m) wind vectors $\overrightarrow{u_{10}}$ used from the ECWMF ERA5-Land reanalysis[6]. These values are common global approximations in lieu of more accurate local values[26]. Here we report the time-averaged magnitude of the saturated flux, $|\overrightarrow{q_s}| = \sum_N |\overrightarrow{Q_s}|/N$, where N is the number of hours in the period 1950-2024. This analysis was carried out in Python with xarray[42] and Dask[43].

M4. Flux directionality

The flux directionality, or so-called "RDP/DP" (resultant drift potential over drift potential), is defined as $|\sum_N \overrightarrow{Q_s}|/\sum_N |\overrightarrow{Q_s}|$, where N is the number of hours in the period 1950-2024, where values are defined between 0 and 1, where 1 indicates perfectly unidirectional saturated sand transport[26].

M5. Aridity and saturated flux inequality

Seeking a parsimonious inequality relating the Aridity Index AI and the time-averaged magnitude of the saturated flux, $|\overrightarrow{q_s}|$ which captures the most dune-present land but least dune-present land, we find values for A and B in the inequality $\log_{10} AI < A|\overrightarrow{q_s}| + B$, using the logarithm of AI since many dunes exist in the lower tail of the AI distribution (Extended Data Fig. 4c). The elbow of the relationship between the fractional cover of land where this inequality is satisfied, AI is defined, and dunes exists, $\hat{C}_D$, and where they do not, $\hat{C}_L$, can be defined as $\max_{A,B}|\hat{C}_L - \hat{C}_D|/\sqrt{2}$, since $|\hat{C}_L - \hat{C}_D|/\sqrt{2}$ is the distance from, and normal to, $\hat{C}_L = \hat{C}_D$. The values $A = 10^{-11/5}$ and $B = 4/5$ allow the inequality to capture (where AI is defined) 93% of land where dunes are present and leave out 81% of land where they are not.

M6. Flux divergence

The saturated flux divergence $\nabla \cdot \overrightarrow{q_s}$ (m/s) is derived from the time-averaged volumetric saturated sand flux $\overrightarrow{q_s}$, defined in latitude ϕ (°), longitude λ (°) grid as,

$$\nabla \cdot \overrightarrow{q_s} = \frac{|\overrightarrow{q_s}|}{R\cos\phi}\left(\frac{\partial}{\partial\lambda}\cos\angle\overrightarrow{q_s} + \frac{\partial}{\partial\phi}(\sin\angle\overrightarrow{q_s}\cos\phi)\right),$$

where Earth's radius R = 6,371 km and the $\angle$ symbol denotes the vector direction.

M7. Surficial lithology

The aeolian sediment surficial lithology data used in this study is from the previously published "Africa Surface Lithology"[14]. Here we coarsen the dataset from 90 arcseconds to a 0.1° grid co-located with the ERA5-Land reanalysis grid.

M8. Migration direction

The signed direction dunes migrate α_T is calculated as 90° from the bed-mode migration instability crest orientation α_H in the positive net across-crest transport direction[26]. The value for α_H is the one which maximises gross bedform normal flux[44] calculated as per the Methods M3 & M4, however the wind vectors $\overrightarrow{u_{10}}$ are replaced by $\overrightarrow{u_c}$ (m/s) to accommodate for the speed-up effect of winds at dune crests relative to flat ground where,

$$|\overrightarrow{u_c}| = |\overrightarrow{u_{10}}|(1 + \beta \mathrm{A}|\sin(\angle\overrightarrow{u_{10}} - \alpha_H)|),$$

and β = 6, the speed-up sensitivity to dune aspect ratio A = 2/15, are assumed.

M9. Barchan dune distribution

The spatial distribution of barchan dunes used in this study is from a previously published AI-generated 30-arcsecond dataset of global dune morphologies[29]. There were some spurious gridded patterns indicating dune presence which we removed manually before analysis. Relative to our manual dataset, this dataset has a precision of 96.5% and recall of 60.4% for dune identification. We coarsened where this dataset predicted 'barchan' and 'superbarchan' dunes, where we have manually identified dunes, and where the Aridity Index AI<0.05, to a 0.1° grid co-located with the ERA5-Land reanalysis grid to best predict active barchan dune distribution.

Data availability

The global dune map can be accessed at https://github.com/geomorphlab/dune-world (NOTE: Zenodo DOI will be provided on acceptance). The ECWMF ERA5-Land[6] hourly data can be accessed at https://doi.org/10.24381/cds.e2161bac. The ESA Copernicus 30-m DSM[7] can be accessed at https://doi.org/10.5069/G9028PQB. The Aridity Index[5] data can be accessed at https://doi.org/10.6084/m9.figshare.7504448. The predicted barchan dune distribution[29] data can be accessed at https://doi.org/10.5281/zenodo.13907012. The INQUA Dune Atlas[15] data can be accessed at https://doi.org/10.1016/j.quaint.2015.10.044.

Code availability

The python code to reproduce this study can be accessed at https://github.com/geomorphlab/dune-world (NOTE: Zenodo DOI will be provided on acceptance).

References

1. Vimpere, L. (2024). Parabolic dune distribution, morphology and activity during the last 20,000 years: A global overview. *Earth Surface Processes and Landforms*, *49*(1), 117-146.
2. Pavlov, B., Konyushkov, D., Khokhlov, S., & Evgrafov, S. (2023). Aeolian Sand Dunes in the Permafrost Zone of Russia. In *Sand Dunes of the Northern Hemisphere: Distribution, Formation, Migration and Management* (pp. 202-218). CRC Press.
3. Hayward, R. K., Mullins, K. F., Fenton, L. K., Hare, T. M., Titus, T. N., Bourke, M. C., ... & Christensen, P. R. (2007). Mars global digital dune database and initial science results. *Journal of Geophysical Research: Planets*, *112*(E11).
4. Kocurek, G., & Lancaster, N. (1999). Aeolian system sediment state: theory and Mojave Desert Kelso dune field example. *Sedimentology*, *46*(3), 505-515.
5. Zomer, R. J., Xu, J., & Trabucco, A. (2022). Version 3 of the global aridity index and potential evapotranspiration database. *Scientific Data*, *9*(1), 409.
6. Muñoz-Sabater, J., Dutra, E., Agustí-Panareda, A., Albergel, C., Arduini, G., Balsamo, G., ... & Thépaut, J. N. (2021). ERA5-Land: A state-of-the-art global reanalysis dataset for land applications. *Earth system science data*, *13*(9), 4349-4383.
7. European Space Agency (2024). *Copernicus Global Digital Elevation Model*. Distributed by OpenTopography.
8. Wang, X., Chen, F., Hasi, E., & Li, J. (2008). Desertification in China: an assessment. *Earth-Science Reviews*, *88*(3-4), 188-206.
9. Thomas, D. S., Knight, M., & Wiggs, G. F. (2005). Remobilization of southern African desert dune systems by twenty-first century global warming. *Nature*, *435*(7046), 1218-1221.
10. Gunn, A., East, A., & Jerolmack, D. J. (2022). 21st-century stagnation in unvegetated sand-sea activity. *Nature Communications*, *13*(1), 3670.
11. Baas, A. C., & Delobel, L. A. (2022). Desert dunes transformed by end-of-century changes in wind climate. *Nature Climate Change*, *12*(11), 999-1006.
12. Gunn, A. (2023). Formation and reorganization time scales of aeolian landscapes. *Geology*, *51*(4), 351-355.
13. Wasson, R. J., & Hyde, R. (1983). Factors determining desert dune type. *Nature*, *304*(5924), 337-339.
14. Sayre, R. G., Comer, P., Hak, J., Josse, C., Bow, J., Warner, H., ... & Waruingi, L. (2013). A new map of standardized terrestrial ecosystems of Africa. *African Geographical Review*.
15. Lancaster, N., Wolfe, S., Thomas, D., Bristow, C., Bubenzer, O., Burrough, S., ... & Zárate, M. (2016). The INQUA dunes atlas chronologic database. *Quaternary International*, *410*, 3-10.
16. Bagnold, R. A. (1941). *The physics of blown sand and desert dunes*. Courier Corporation.
17. Martin, R. L., & Kok, J. F. (2017). Wind-invariant saltation heights imply linear scaling of aeolian saltation flux with shear stress. *Science Advances*, *3*(6), e1602569.
18. Ash, J. E., & Wasson, R. J. (1983). Vegetation and sand mobility in the Australian desert dunefield. *Zeitschrift fur Geomorphologie*, *45*(Supp.), 7-25.
19. Nield, J. M., & Baas, A. C. (2008). The influence of different environmental and climatic conditions on vegetated aeolian dune landscape development and response. *Global and Planetary Change*, *64*(1-2), 76-92.
20. Mckenna Neuman, C. (2003). Effects of temperature and humidity upon the entrainment of sedimentary particles by wind. *Boundary-Layer Meteorology*, *108*(1), 61-89.
21. Parteli, E. J., Durán, O., & Herrmann, H. J. (2007). Minimal size of a barchan dune. *Physical Review E—Statistical, Nonlinear, and Soft Matter Physics*, *75*(1), 011301.
22. Alkalla, J., Narteau, C., Rozier, O., Vérité, J., & Courrech du Pont, S. (2025). Steady-state dune morphodynamics through the barchan-parabolic transition. *Journal of Geophysical Research: Earth Surface*, *130*(4), e2024JF008220.
23. Lancaster, N. (1988). Development of linear dunes in the southwestern Kalahari, southern Africa. *Journal of Arid Environments*, *14*(3), 233-244.
24. Hesp, P. A., & Thom, B. G. (1990). Geomorphology and evolution of active transgressive dunefields. In *Coastal dunes. form and process* (pp. 253-288).
25. Chanteloube, C., Barrier, L., Derakhshani, R., Gadal, C., Braucher, R., Payet, V., ... & Narteau, C. (2022). Source-to-sink aeolian fluxes from arid landscape dynamics in the Lut Desert. *Geophysical Research Letters*, *49*(4), e2021GL097342.
26. Courrech Du Pont, S., Rubin, D. M., Narteau, C., Lapôtre, M. G., Day, M., Claudin, P., ... & Wiggs, G. F. (2024). Complementary classifications of aeolian dunes based on morphology, dynamics, and fluid mechanics. *Earth-Science Reviews*, *255*, 104772.
27. Rubanenko, L., Gunn, A., Pérez-López, S., Fenton, L. K., Ewing, R. C., Soto, A., & Lapôtre, M. G. A. (2023). Global surface winds and aeolian sediment pathways on Mars from the morphology of barchan dunes. *Geophysical Research Letters*, *50*(18), e2022GL102610.
28. Shao, Y., & Lu, H. (2000). A simple expression for wind erosion threshold friction velocity. *Journal of Geophysical Research: Atmospheres*, *105*(D17), 22437-22443.
29. Zheng, Z., Zhang, X., Li, J., Ali, E., Yu, J., & Du, S. (2024). Global perspectives on sand dune patterns: Scale-adaptable classification using Landsat imagery and deep learning strategies. *ISPRS Journal of Photogrammetry and Remote Sensing*, *218*, 781-801.
30. Yizhaq, H., Ashkenazy, Y., & Tsoar, H. (2007). Why do active and stabilized dunes coexist under the same climatic conditions? *Physical Review Letters*, *98*(18), 188001.
31. Durán, O., & Herrmann, H. J. (2006). Vegetation against dune mobility. *Physical Review Letters*, *97*(18), 188001.
32. Fisher, A., & Hesse, P. P. (2019). The response of vegetation cover and dune activity to rainfall, drought and fire observed by multitemporal satellite imagery. *Earth Surface Processes and Landforms*, *44*(15), 2957-2967.
33. Hesse, P. P. (2016). How do longitudinal dunes respond to climate forcing? Insights from 25 years of luminescence dating of the Australian desert dunefields. *Quaternary International*, *410*, 11-29.

34. Burrell, A. L., Evans, J. P., & De Kauwe, M. G. (2020). Anthropogenic climate change has driven over 5 million km^2 of drylands towards desertification. *Nature Communications*, *11*(1), 3853.
35. Ren, H., Gao, X., Zhao, Y., Lei, J., De Maeyer, P., & De Wulf, A. (2024). Strong-wind events control barchan dune migration. *Communications Earth & Environment*, *5*(1), 278.
36. Hunter, R. E., & Rubin, D. M. (1983). Interpreting cyclic crossbedding, with an example from the Navajo Sandstone. In *Developments in sedimentology* (Vol. 38, pp. 429-454). Elsevier.
37. Nanson, G. C., Chen, X. Y., & Price, D. M. (1995). Aeolian and fluvial evidence of changing climate and wind patterns during the past 100 ka in the western Simpson Desert, Australia. *Palaeogeography, Palaeoclimatology, Palaeoecology*, *113*(1), 87-102.
38. Cousins, D., Kocurek, G., Al Kindi, M., Al Mashaykhi, O., Hern, C., Macaulay, C., ... & Thompson, M. (2025). Mineralogical characterisation of aeolian sands using multispectral satellite datasets: Implications for dune field evolution, Wahiba Dune Field, Oman. *Earth Surface Processes and Landforms*, *50*(6), e70064.
39. Chiang, J. C. (2009). The tropics in paleoclimate. *Annual Review of Earth and Planetary Sciences*, *37*(1), 263-297.
40. Campos, J. C., & Brito, J. C. (2018). Mapping underrepresented land cover heterogeneity in arid regions: the Sahara-Sahel example. *ISPRS Journal of Photogrammetry and Remote Sensing*, *146*, 211-220.
41. Liu, Y., Wang, Y. S., & Shen, T. (2019). Spatial distribution and formation mechanism of aeolian sand in the middle reaches of the Yarlung Zangbo River. *Journal of Mountain Science*, *16*(9), 1987-2000.
42. Hoyer, S., & Hamman, J. (2017). xarray: ND labeled arrays and datasets in Python. *Journal of Open Research Software*, *5*(1), 10-10.
43. Rocklin, M. (2015). Dask: Parallel computation with blocked algorithms and task scheduling. In *SciPy* (pp. 126-132).
44. Rubin, D. M., & Hunter, R. E. (1987). Bedform alignment in directionally varying flows. *Science*, *237*(4812), 276-278.
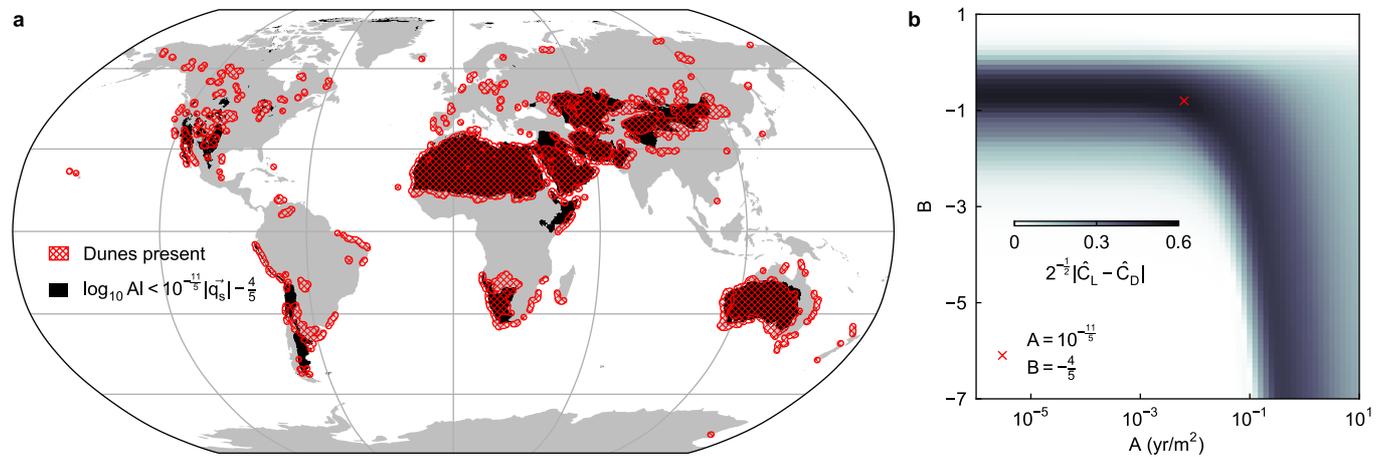
Acknowledgements

Ethics declarations

The author declares no competing interests.

Extended Data

Extended Data Fig. 1: Aridity and saturated flux inequality for dune presence. a, Dune presence hatched in red on a world map (ESRI:54030) where $\log_{10} AI < 10^{-11/5}|\vec{q_s}| - 4/5$ (black). **b**, The $\hat{C}_L = \hat{C}_D$-normal distance between $\hat{C}_L = \hat{C}_D$ and $\hat{C}_L(A,B), \hat{C}_D(A,B)$, $|\hat{C}_L - \hat{C}_D|/\sqrt{2}$, where $\hat{C}_D$ and $\hat{C}_L$ are the fraction of land that satisfies $\log_{10} AI < A|\vec{q_s}| + B$ where dunes are, and are not, present, respectively (Methods M5), and its maximum (red cross).
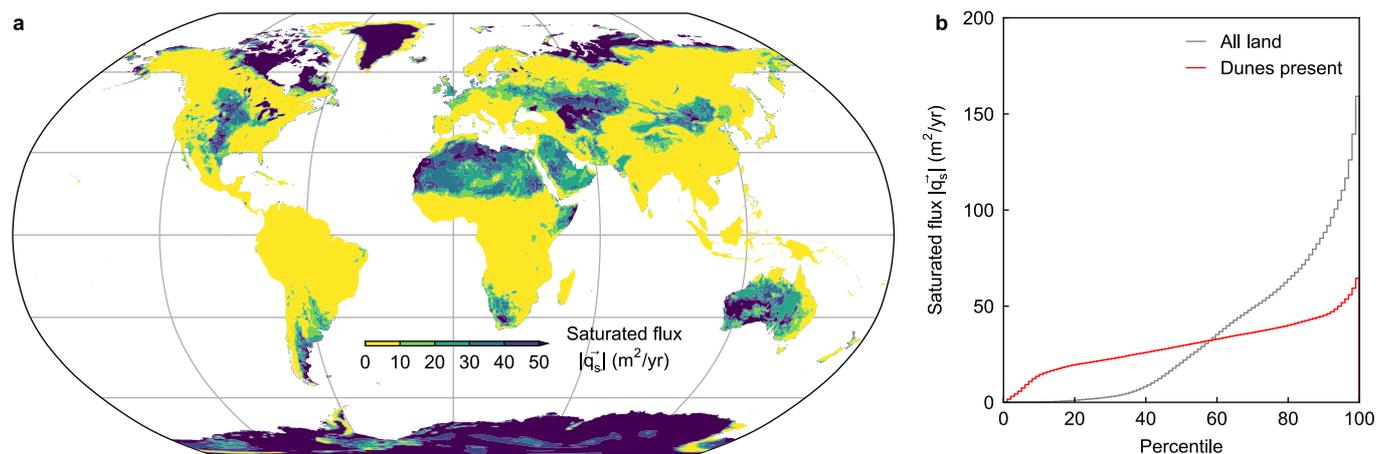
Extended Data Fig. 2: Saturated sand flux percentiles. a, World map (ESRI:54030) of the average saturated sand flux magnitude $|\vec{q_s}|$ (m^2/yr). **b**, The area-weighted percentiles for land (grey) and regions where dunes are present (red).
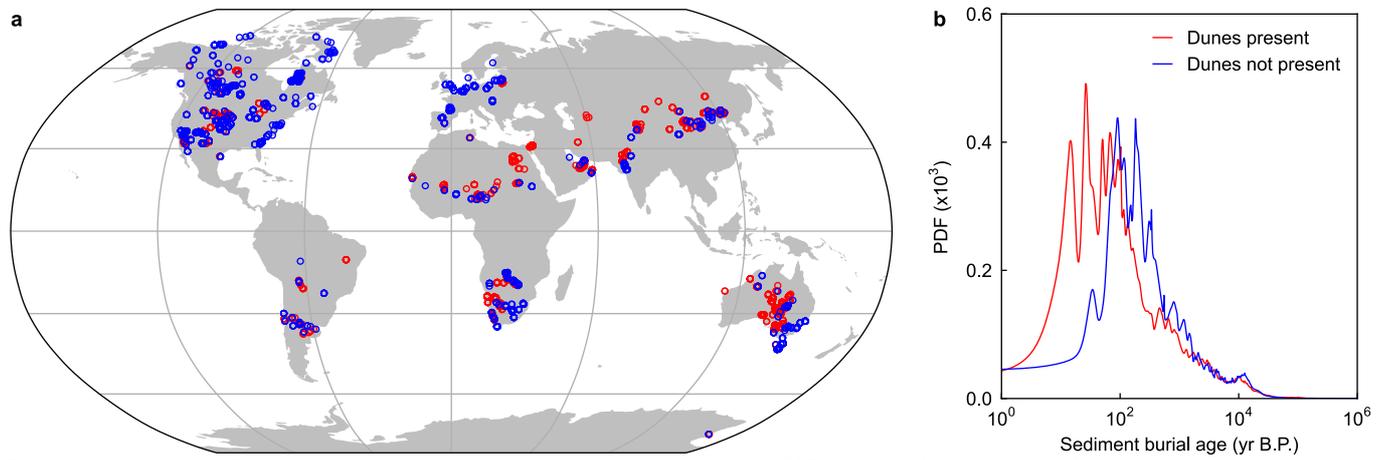
Extended Data Fig. 3: Reported aeolian sediment burial ages. a, World map (ESRI:54030) of the locations of luminescence and radiocarbon dating burial ages in aeolian sediments from the INQUA Dune Atlas[15] where errors are reported, where dunes with surface morphologies are present (red) or not (blue). **b**, The probability distribution functions, i.e., the simple-mean gaussian mixture, of all burial ages where dunes are present (red; N=2,295) or not (blue; N=2,097). Note that, in lieu of a detailed analysis of each specific age, this simplistic approach neglects contextual information about samples such as their depth or stratigraphic unit.
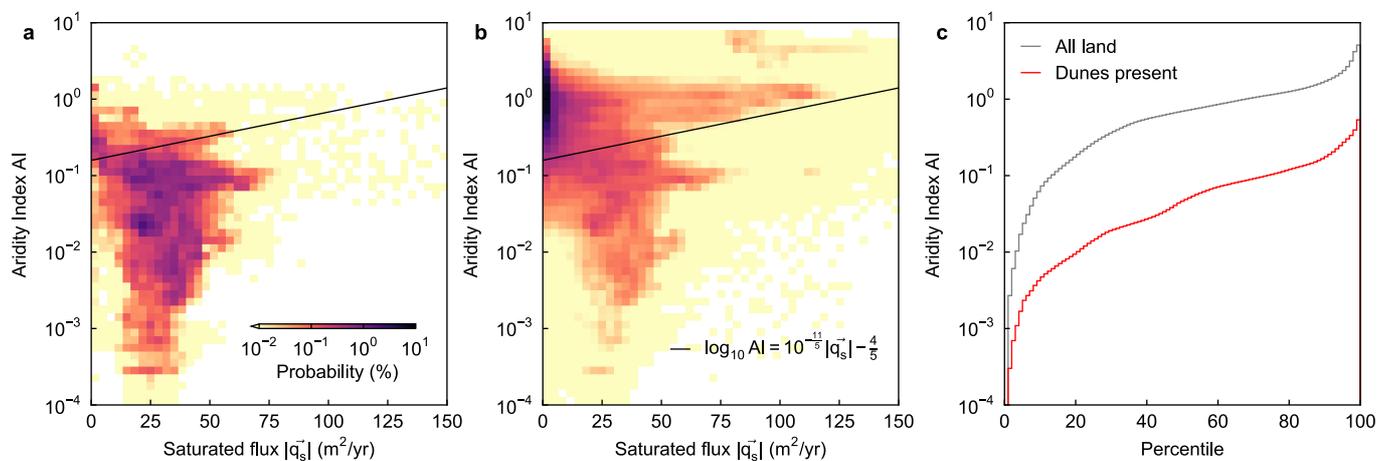
Extended Data Fig. 4: Likelihood of aridity and saturated flux. a, The joint area-weighted probability (log-scale) of Aridity Index AI and average saturated sand flux magnitude $|\vec{q_s}|$ (m²/yr) where dunes are present, and **b**, for all land, with the relation $\log_{10} AI = 10^{-11/5}|\vec{q_s}| - 4/5$ (Methods M5) shown in black. **c**, The area-weighted percentiles for land (grey) and regions where dunes are present (red).

Supplementary Information for "The distribution of Earth's wind-blown sand dunes"

Andrew Gunn[1,*]

[1]School of Earth, Atmosphere & Environment, Monash University, Clayton, Victoria, Australia

[*]a.gunn@monash.edu

Supplementary Text 1

Many other secondary source maps were used to develop the map used in this study[1-29]. This text section provides further details on the manual mapping of dune presence.

Omissions

- The map is void where ERA5-Land reanalysis data is not provided, i.e., any 0.1°x0.1° grid cell where the area is majority water (except some lakes) and therefore omits many coastal dunes.
- Some dunes are too small (in height or planform) to observe at the mapping scale used.
- Some dunes are presently obscured by thick vegetation and cannot be discerned with the datasets used (e.g., COP30 is a Digital Surface Model, not a Digital Terrain Model). In some parts of Earth better datasets which would result in a more comprehensive map could be used (e.g., USGS 3DEP DTM), however, to ensure an unbiased map the same globally available datasets were used everywhere.
- Some aeolian dune fields can be identified but their surface expression is too modest, altered, or complex to identify a morphology, therefore they are omitted. This is particularly true for relict dunes. Some example regions are the Pampas, Kalahari, Low Qoz, Qoz Dango, Hausaland, Nara, East Caspian, Lapland, North Europe, North America, and Siberia.

New additions

This map includes dunes in the following regions which, to the best of the author's knowledge, are not identified in other published maps including those used as secondary sources for this study:

- Nenetsia, Russia
- East of the Lut, Iran
- Afghanistan border with Tajikistan & Uzbekistan
- North-facing Himalaya, Tibet
- Sevrei, Mongolia
- Töv, Mongolia
- West Tabuk, Saudi Arabia
- Samara, Kazakhstan
- Jubaland coast, Somalia
- Senegal-Gambia border
- Between Bir Anzerane & Awsard, Western Sahara
- El Hank escarpment, Mauritania
- Downwind of Bel Bouna, Mauritania
- Djebel Ouarkziz, Algeria
- Between Taoundart & Amesmessa, Algeria
- Western Tazrouk Province, Algeria
- Western Tibetsi Mountains, Chad
- Around Sabkhat al Qunnayyin, Libya
- Between Ghurd as Sara & Al Jawf, Libya
- Eastern side of Jabal Nuqayy, Libya

Notes on definition of marginal dunes

Free elongating dunes are only classified if they have a sharp crest. Often there are mounds of sand in the lee of obstacles without a crest; we have not classified these as dunes. Similarly, we have not classified mounds of free sand without a clear wind-driven asymmetry in morphology as dunes. These, in some cases, may be dome dunes, however it is not possible to definitively distinguish them as aeolian.

Parabolic dunes have tremendous variety in morphology. This is partially because; they can form in unimodal winds with a variety of dispersions, have various stabilising forces (i.e., ice, vegetation, microbial mats, etc.), and, since they often are on the fringes of aeolian activity, can reactivate and degrade in unexpected ways on a variety of timescales from seasonal to Milankovitch. We have erred on a bullish identification of these dunes. We have, however, maintained a consistent approach to not classifying 'blowouts' without a clear downwind crest, i.e., an eroding sand patch surrounded by vegetation (or another stabilising force) containing no discernible bedforms, as dunes. These are prevalent in coastal settings and the Pampas.

Superimposed dunes with unique morphologies can prevail when either all morphologies are active, only some are active, or none. When none are active, and topography is degraded somewhat, these dunes can be difficult to identify. Therefore, there may be some locations where these are not included by mistake.

In some locations, particularly large ergs, there can be fields of consistently patterned dunes that, despite not displaying slipfaces, appear with context to be mature and free, akin to dome dunes but with high sand supply. We have classified these as dunes however they do not fit within a typical dune classification scheme. We have distinguished these from sand drifts which, despite having fine-scale micro-relief patch patterns, are not considered dunes, using historical Landsat imagery to assess their migration speed. A clear example of this distinction is seen between the Zaltan & Calanscio dune fields.

Sometimes there are clear aeolian patterns on surfaces (e.g., intermittently wet lake beds) that are not dunes. They can form for various reasons, such as through feedbacks between wind and vegetation or evaporation, but have not classified as dunes as they are not topographic forms.

There are certainly places which we have indicated dunes that would be up for expert debate, e.g., subtle relict nail dunes along the Warrego River, Australia, the crests of eroding hills south of the Nafusa Mountains, Libya, or slip faces developing upwind of the stoss of obstacles west of Mont Touside, Chad. These surmount to a negligible fraction of the dataset (<0.1%) so should not meaningfully impact the results.

Supplementary Text 2

Past studies have introduced Mobility Indices for dune activity which have proved extremely useful for distilling the competing effects of wind and vegetation on dune activity[30-37]. These include myriad parameterisations for important hydroclimate and wind climate properties, such as the percentage of time wind exceed a threshold for sand transport[30,32,34], the mean wind speed raised to some power[31,32], the "RDP/DP"[35] (Methods M4), different flavours of the Aridity Index[30,36], and the ratio of actual to potential evapotranspiration[32]. Some also include reasonable memory effects which parameterise the influence of drought[32] or existing non-equilibrium vegetation[37]. Threshold values for these Mobility Indices are proposed which delineate when dunes become active or should be present[30-34]. Here we compare the precision and recall of the relation $\log_{10} AI < 10^{-11/5}|\vec{q_s}| - 4/5$ to commonly employed past criteria (Supplementary Table 1).

In order to make this comparison, we have made some minor assumptions. Lancaster[30] proposed that dune activity occurs when $W/AI > 50$, where W (%) is the percentage of time $|\vec{u_{10}}| > 4.5$ (m/s) and AI is the Aridity Index, where calculated in the Thornthwaite method—we assume the AI is consistent with the values used in this study. Ash & Wasson[32] proposed that dune activity occurs when $|\vec{u_{10}}|^4/(AET/PET) > 10^4/3.8$ or $W^2/(AET/PET) > 10^4/5$, where AET is the actual evapotranspiration and PET is the potential evapotranspiration—we approximate AET/PET as AI. Thomas et al.[31] proposed that dune activity occurs when $|\vec{u_{10}}|^3/AI > 70$, with a month-long memory effect due to drought—we neglect the memory effect.

Supplementary Table 1 shows that all other methods tested here have reduced precision relative to the relation in this study, apart from $|\vec{u_{10}}|^4/(AET/PET) > 10^4/3.8$ which has significantly worse recall. Note that the reduced recall relative to some other studies should be weighed against the increase in precision: since dune grid cells only account for 7.8% of the land surface, precision scores are far harder to increase relative to recall. Also note that, as discussed elsewhere in the study, all precisions are relatively low due to the role that other boundary conditions (i.e., flux divergence and sediment source location) play in the distribution of dunes, and recall is lower since relict dunes make up a small fraction of the dataset.

Supplementary Table 1

Study	Criterion	Precision	Recall
Lancaster (1988)[30]	$W/AI > 50$	26	96
Thomas et al. (2005)[31]	$|\vec{u_{10}}|^3/AI > 70$	23	98
Ash & Wasson (1983)[32]	$|\vec{u_{10}}|^4/(AET/PET) > 10^4/3.8$	41	72
	$W^2/(AET/PET) > 10^4/5$	28	93
Muhs & Holliday (1995)[33]	$AI < 0.35$	25	98
Wasson (1984)[34]	$0.13W + \ln AI^{-1} > 1/0.21$	27	90
This study	$\log_{10} AI < 10^{-11/5}|\vec{q_s}| - 4/5$	32	93

Supplementary Table 1: Precision and recall of mobility indices. Reported threshold criterion for dune mobility in other studies (Supplementary Text 2), and this study (Methods M5), and their area-weighted precision and recall scores (%).

References

1. Zheng, Z., Zhang, X., Li, J., Ali, E., Yu, J., & Du, S. (2024). Global perspectives on sand dune patterns: Scale-adaptable classification using Landsat imagery and deep learning strategies. *ISPRS Journal of Photogrammetry and Remote Sensing, 218*, 781-801.
2. Gunn, A., Casasanta, G., Di Liberto, L., Falcini, F., Lancaster, N., & Jerolmack, D. J. (2022). What sets aeolian dune height? *Nature Communications, 13*(1), 2401.
3. Lu, Q., Gaur, M. K., & Squires, V. R. (Eds.). (2023). *Sand Dunes of the Northern Hemisphere: Distribution, Formation, Migration and Management, Volume 1*. CRC Press.
4. Lancaster, N. (2013). *Geomorphology of desert dunes*. Routledge.
5. Zhang, Z., Ma, P., La, Z., Zhang, Y., & Liang, A. (2023). Aeolian sediment provenance and transport in the upper and middle reaches of the Yarlung Zangbo River, Tibet Plateau. *Basin Research, 35*(2), 762-783.
6. Liu, Y., Wang, Y. S., & Shen, T. (2019). Spatial distribution and formation mechanism of aeolian sand in the middle reaches of the Yarlung Zangbo River. *Journal of Mountain Science, 16*(9), 1987-2000.
7. Dong, Z., Hu, G., Qian, G., Lu, J., Zhang, Z., Luo, W., & Lyu, P. (2017). High-altitude aeolian research on the Tibetan Plateau. *Reviews of Geophysics, 55*(4), 864-901.
8. Doody, J. P. (Ed.). (1991). *Sand dune inventory of Europe*. JNCC/EUCC.
9. Muhs, D. R. (2017). Evaluation of simple geochemical indicators of aeolian sand provenance: Late Quaternary dune fields of North America revisited. *Quaternary Science Reviews, 171*, 260-296.
10. Lancaster, N., & Hesp, P. (Eds.). (2020). *Inland Dunes of North America*. Springer.
11. Latrubesse, E. M., Stevaux, J. C., Cremon, E. H., May, J. H., Tatumi, S. H., Hurtado, M. A., ... & Argollo, J. B. (2012). Late Quaternary megafans, fans and fluvio-aeolian interactions in the Bolivian Chaco, Tropical South America. *Palaeogeography, Palaeoclimatology, Palaeoecology, 356*, 75-88.
12. Baas, A. C., & Delobel, L. A. (2022). Desert dunes transformed by end-of-century changes in wind climate. *Nature Climate Change, 12*(11), 999-1006.
13. Vimpere, L. (2024). Parabolic dune distribution, morphology and activity during the last 20 000 years: A global overview. *Earth Surface Processes and Landforms, 49*(1), 117-146.
14. Wolfe, S. (2025). Paleowind directions in northern North America from stabilized sand dunes [Dataset]. *Natural Resources Canada.*
15. Sayre, R. G., Comer, P., Hak, J., Josse, C., Bow, J., Warner, H., ... & Waruingi, L. (2013). A new map of standardized terrestrial ecosystems of Africa. *African Geographical Review.*
16. Wang, J., Wang, Y., Yan, C., & Qi, Y. (2013). 1: 100,000 desert (sand) distribution dataset in China. *Center NTPD, editor.*
17. Geoscience Australia (2006). GEODATA TOPO 250K Series 3 [Dataset]. *Geoscience Australia, Canberra.*
18. Lancaster, N., Wolfe, S., Thomas, D., Bristow, C., Bubenzer, O., Burrough, S., ... & Zárate, M. (2016). The INQUA dunes atlas chronologic database. *Quaternary International, 410*, 3-10.
19. Hesse, P. P. (2010). The Australian desert dunefields: formation and evolution in an old, flat, dry continent. *Geological Society, London, Special Publications, 346*(1), 141-164.
20. Miguel, L. L. A. J., & Castro, J. W. A. (2018). Aeolian dynamics of transgressive dunefields on the southern Mozambique coast, Africa. *Earth Surface Processes and Landforms, 43*(12), 2533-2546.
21. Warren, A. (1970). Dune trends and their implications in the central Sudan. *Z. Geomorphol. Suppl, 10*, 154-180.
22. Crouvi, O., Schepanski, K., Amit, R., Gillespie, A. R., & Enzel, Y. (2012). Multiple dust sources in the Sahara Desert: The importance of sand dunes. *Geophysical Research Letters, 39*(13).
23. Hu, Z., Gao, X., Lei, J., & Zhou, N. (2021). Geomorphology of aeolian dunes in the western Sahara Desert. *Geomorphology, 392*, 107916.
24. Campos, J. C., & Brito, J. C. (2018). Mapping underrepresented land cover heterogeneity in arid regions: the Sahara-Sahel example. *ISPRS Journal of Photogrammetry and Remote Sensing, 146*, 211-220.
25. Maman, S., Porat, N., Meged, C., Blumberg, D. G., Tsoar, H., Mamedov, B., & Roskin, J. (2023). The Karakum and Kyzylkum Sand Seas. *Sand Dunes of the Northern Hemisphere: Distribution, Formation, Migration and Management: Volume 2: Characteristics, Dynamics and Provenance of Sand Dunes in the Northern Hemisphere*, 253.

26. Al-Dousari, A., Awadh, S., Bamousa, A., Al-Awadhi, J., Al-Dousari, N., Al-Rawi, M., ... & William, T. (2023). Barchan dunes properties in the Middle East. In *Sand Dunes of the Northern Hemisphere: Distribution, Formation, Migration and Management* (pp. 129-149). CRC Press.

27. Embabi, N. S. (2023). Barchan Dunes in Egypt Distribution and Formation. In *Sand Dunes of the Northern Hemisphere: Distribution, Formation, Migration and Management* (pp. 150-180). CRC Press.

28. Goudie, A. S., Goudie, A. M., & Viles, H. A. (2021). Dome dunes: Distribution and morphology. *Aeolian Research*, *51*, 100713.

29. Abbasi, H. R., Opp, C., Groll, M., Rohipour, H., & Gohardoust, A. (2019). Assessment of the distribution and activity of dunes in Iran based on mobility indices and ground data. *Aeolian Research*, *41*, 100539.

30. Lancaster, N. (1988). Development of linear dunes in the southwestern Kalahari, southern Africa. *Journal of Arid Environments*, *14*(3), 233-244.

31. Thomas, D. S., Knight, M., & Wiggs, G. F. (2005). Remobilization of southern African desert dune systems by twenty-first century global warming. *Nature*, *435*(7046), 1218-1221.

32. Ash, J. E., & Wasson, R. J. (1983). Vegetation and sand mobility in the Australian desert dunefield. *Zeitschrift fur Geomorphologie*, *45*(Supp.), 7-25.

33. Muhs, D. R., & Holliday, V. T. (1995). Evidence of active dune sand on the Great Plains in the 19th century from accounts of early explorers. *Quaternary Research*, *43*(2), 198-208.

34. Wasson, R. J. (1984). Late Quaternary palaeoenvironments in the desert dunefields of Australia. In *Late Cainozic palaeoclimates of the Southern Hemisphere. International symposium held by the South African Society for Quaternary Research; Swaziland* (pp. 419-432).

35. Tsoar, H. (2005). Sand dunes mobility and stability in relation to climate. *Physica A: Statistical Mechanics and its Applications*, *357*(1), 50-56.

36. Talbot, M. (1984). Late Pleistocene rainfall and dune building in the Sahel. In *Palaeoecology of Africa and the surrounding Islands*, volume 16 (pp. 203-214).

37. Yizhaq, H., Ashkenazy, Y., & Tsoar, H. (2007). Why do active and stabilized dunes coexist under the same climatic conditions? *Physical Review Letters*, *98*(18), 188001.